Initial stages of square lattice stacks of CH_4/MgO(001)

L. W. Bruch*
Department of Physics, University of Wisconsin-Madison, Madison, Wisconsin 53706, USA

J. Z. Larese†
Chemistry Department, University of Tennessee, Knoxville, Tennessee 37996, USA

(Received 7 November 2011; revised manuscript received 19 December 2011; published 3 January 2012)

Calculations of monolayer and bilayer lattices of methane on MgO(001) are reported for a spherical model of the molecule. The observed stability of $c(2 \times 2)$ [also termed $(\sqrt{2} \times \sqrt{2})$R45°] commensurate square monolayer and bilayer lattices is reproduced with a surface energy corrugation that implies a large gap in the monolayer phonon density of states of the commensurate CH_4. This gap is present in the incoherent inelastic neutron scattering measurements reported here.

DOI: 10.1103/PhysRevB.85.035401 PACS number(s): 68.43.Pq, 78.70.Nx

I. INTRODUCTION

Multilayer films of CH_4/MgO(001) and CD_4/MgO(001) have been the subject of extensive measurements because they appeared very suitable for studies of surface-induced melting, as reviewed by Bienfait and Gay.[1] The initial stages of the film growth continue to attract attention in the *a priori* quantum theory of catalytic processes.[2,3] Many film parameters are known and the first few layers are commensurate square solid lattices.

The stability of the square monolayer and bilayer lattices also is intrinsically interesting. There is six-fold coordination in a monolayer triangular lattice but only four-fold coordination in the monolayer square lattice. While the original observation of the methane commensurate square lattice[4] was not considered to be very remarkable, because the nearest-neighbor separation L_{nn} in the monolayer was only 1% different from that in the ground state of the three-dimensional (3D) solid, the energetics imply an unusual physical adsorption system. To balance the difference in lateral cohesive energy arising from the smaller coordination, the corrugation energy arising from the substrate must be larger than the attractive potential energy of a pair of the molecules. The only other physical adsorption system for which such a large corrugation is known to occur is[5] H_2/NaCl(001). The large corrugation implies a large gap in the monolayer phonon density of states, which indeed is present in the incoherent inelastic neutron scattering data reported in Sec. II B.

The square monolayer has unusual lattice dynamics, because the interactions with next-nearest neighbors cause the smallest in-plane vibrational frequency to be at the Brillouin zone edge, in contrast to the minimum at the Brillouin zone center for triangular lattices. The most likely competing commensurate-incommensurate transition in the monolayer is[6] a first-order transition from square to compressed triangular lattice, although a continuous transition to a uniaxially compressed lattice of heavy walls[7] is favored at large corrugations.

Because so much is known about the methane/MgO system, it is reasonable to expect that an atomic scale model calculation will reproduce the remarkable features of the monolayer domain. Complications arise from the molecular character of the adsorbate and from the significant role of quantum zero-point energies in the low-temperature solids. There is orientational ordering in the very-low-temperature monolayer solid.[8] However, over much of the monolayer phase diagram, the molecule is in a state of nearly free rotation and a spherical molecule approximation is sufficient to reproduce most of the observations. Quasiharmonic lattice dynamics suffice to evaluate the zero-point energy effects.

The organization of this paper is as follows. Section II contains a summary of the experimental data and Sec. III contains the formulation of the calculations. Results of the calculations are presented in Sec. IV and discussed in Sec. V. Concluding remarks are presented in Sec. VI. The Appendix describes an extension of the Novaco-McTague perturbation theory[9] to a strongly corrugated monolayer. Supplementary material has been deposited in Ref. 10.

II. SUMMARY OF THE EXPERIMENTAL DATA

A. Review of previous data

The degree of rotational ordering of the monolayer solid of CH_4/MgO(001) was measured[8,11] using quasielastic neutron scattering over a temperature range from 1.5 to 50 K. The molecule is rotationally ordered below 15 K, rotationally disordered at 20 K, and essentially has a free rotation above 40 K. The monolayer melts[12] near 80 K.

The structure of thin methane films was determined in several diffraction experiments. Early neutron scattering experiments showed[4] that the monolayer and bilayer of CD_4/MgO(001) form commensurate $c(2 \times 2)$ square lattices up to 10 K. Later experiments showed that CD_4 grows as a commensurate square lattice to 3 layers at[8] 50 K and to 4 layers at[13,14] 77 K. Helium atom scattering[15] confirmed that the CH_4/MgO(001) monolayer is a commensurate $c(2 \times 2)$ square lattice at 33–36 K, as shown also at 50 K by low-energy electron diffraction.[16] Adsorption isotherm data[12,13] indicate limited wetting of CH_4/MgO(001) at lower temperatures and that the fourth layer becomes unstable[13] below 40 K.

Integral heats of adsorption q_i for condensation of the monolayer and bilayer CH_4/MgO(001) are known from adsorption isotherms, mostly for the temperature range 70 to 95 K. For the monolayer condensation, Freitag and Larese report[12] $q_1 = 1385 \pm 7$ K and cite Madih[17] for $q_1 = 1590 \pm 50$ K. For the bilayer condensation, they report

$q_2 = 1212 \pm 2$ K and cite Madih for $q_2 = 1219 \pm 6$ K. For comparison, the latent heat of sublimation of 3D CH_4 at very low temperatures is[18] 1126 K.

The results of a direct determination of chemical potential differences at fixed temperature are used here for comparison to calculated stability margins. Freitag and Larese give $\Delta\mu_{12} \equiv \mu_2 - \mu_1 = 260$–$280$ K and $\mu_{3D} - \mu_1 = 350$–370 K for isotherms at 70–87 K, where μ_1, μ_2, and μ_{3D} are the chemical potentials at monolayer, bilayer, and 3D solid condensation, respectively. The difference $\Delta\mu_{12} \simeq 270$ K is much smaller than the value[19] $\Delta\mu_{12} \simeq 650$ K for triangular monolayer and bilayer lattices of CH_4/graphite.

B. Incoherent inelastic neutron scattering

In order to examine the dynamics of the methane monolayer solid, incoherent inelastic neutron scattering (INS) experiments were performed using the H5 triple axis spectrometer at the Brookhaven National Laboratory's High Flux Beam Reactor (HFBR) neutron source. INS offers unrivaled sensitivity for investigating the microscopic dynamics of condensed matter, especially molecular systems containing hydrogen. The spectrometer was configured in an energy-loss, fixed-final energy ($E_f = 14.7$ meV) mode using a Ge(111) monochromator and a PG(002) analyzer, which resulted in an energy resolution (FWHM) of 0.6 meV at the elastic position. The cylindrical, thin-walled, aluminum sample cell was filled with ~10 g of MgO powder. The MgO is comprised of uniform cubic particles ~250 nm in size (edge length) and essentially single facet (100) exposure produced using a patented process developed by Kunnmann and Larese.[20] The powder-averaged INS spectrum shown in Fig. 1 was recorded at 9.0 K at a wave vector transfer $Q = 2.35$ Å^{-1}. The spectra shown in the figure have the response of the MgO substrate (no film adsorbed) subtracted away. As noted above, monolayer methane forms a commensurate $c(2 \times 2)$ phase and the methane coverage investigated here corresponds to 95% of the completed monolayer (100-cm^3 STP, where STP is standard temperature and pressure).

Figure 1 shows that there are essentially no excitations that involve the phonon density of states below about 2.5 meV. The free rotor transition of the molecule at about 1.15 meV is present at higher temperatures but disappears completely below 5 K in INS measurements for monolayer CH_4/MgO(001), Fig. 3 of Ref. 21 and Fig. 3 of Ref. 22 at 1.5 and 4 K.

We summarize some comparisons of the lattice dynamics for adsorption on MgO and on graphite. The nearly dispersionless perpendicular frequency is[15] $\omega_\perp = 7.5$ meV for CH_4/MgO(001) and is[23] $\omega_\perp = 12.5$ meV for CH_4/graphite. For the in-plane phonon motions, the zone-center frequency gap is[24] $\omega_{0,\parallel} = 1.25$ meV for commensurate CD_4/graphite and the lower edge of the density of states is estimated from Fig. 1 to be $\omega_{\min,\parallel} = 2.5$ meV for CH_4/MgO(001).

III. INTERACTION MODELS AND THEORY

The interaction models used here for the stability determinations are empirically based. It is useful to note, though, the status of *a priori* calculations of the molecule-substrate, CH_4-MgO(001), interactions. Drummond *et al.*[2] evaluated the relative energies of methane configurations and concluded that the dipod-down configuration is the most stable, in agreement with the results of rotational tunneling measurements for temperatures below 15 K. Tosoni and Sauer[3] calculated a monolayer adsorption energy of 13.3 kJ mole^{-1} (=138 meV = 1600 K) in good agreement with experimental estimates[12,26] of 120–126 meV. However, the calculated vibration frequencies are[25] about twice the experimental CH_4 results (i.e., a factor of four in the force constant) for the perpendicular vibration $\omega_\perp$ obtained from inelastic helium atom scattering[15] and for the lower edge of the in-plane vibration spectrum $\omega_{\min,\parallel}$ reported in Sec. II B. For the present work, parameters of the CH_4-MgO(001) interaction are based on experimental data for molecules in the monolayer and from an estimate of the London-van der Waals energy for molecules in the second layer of the bilayer solid.

The force constant for perpendicular vibrations is derived from the frequency $\omega_\perp = 7.5$ meV measured by helium scattering[15] for CH_4/MgO(001), which scales to 6.7 meV for CD_4/MgO(001). The interaction of the first-layer molecules with the square substrate lattice is taken to be determined by two parameters V_0 and V_{g0}:

$$V_s(x,y) = V_0 + 2V_{g_0}(\cos g_0 x + \cos g_0 y), \tag{1}$$

where $g_0 = 2\pi/\ell$ with $\ell = 2.98$ Å for MgO(001). The Fourier amplitude V_{g0} determines the energy parameter Ω,

$$\Omega = \hbar g_0 \sqrt{2|V_{g0}|/m}\ , \tag{2}$$

(particles of mass m). Ω is equal to Brillouin zone center frequency gap $\omega_{0\|}$ when the ground state lattice is the $c(2 \times 2)$ commensurate square lattice with one molecule per unit cell. For square lattices $\omega_{0\|}$ is distinct from the minimum in-plane frequency in the Brillouin zone, $\omega_{\min,\parallel}$, which determines the gap in a measured density-of-states spectrum. The two values differ by 10–20% in these calculations for CH_4/MgO(001) and the distinction probably is much larger[6] for a commensurate square lattice of Kr/NaCl(001).

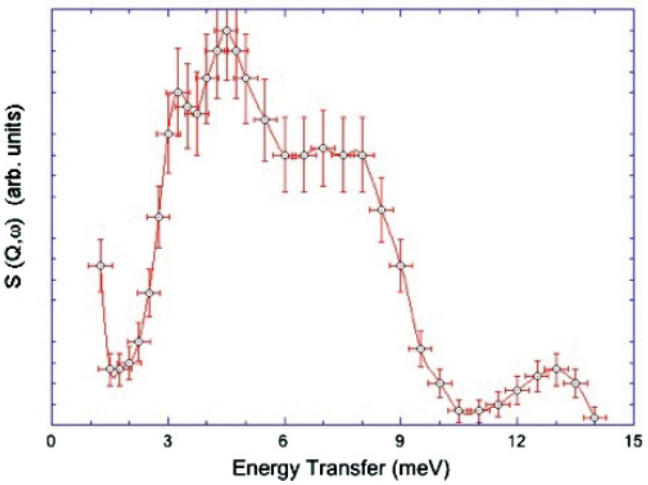

FIG. 1. (Color online) INS difference plot of $S(Q,\omega)$ from 0.95 $c(2 \times 2)$ commensurate monolayer of CH_4 on the MgO(001) surface at $Q = 2.35$ Å^{-1} using the H5 three-axis spectrometer set in the fixed final-energy mode with a resulting energy resolution at the elastic position of 0.6 meV FWHM. $T = 9.0$ K.

The parameters V_0 and V_{g0}, specific to CH_4 adsorption on MgO(001), are set by requiring that the monolayer condenses as a square lattice, rather than a triangular lattice, and that the square bilayer lattice condenses before the chemical potential is increased to the point that a monolayer triangular lattice forms. The model calculations were guided by the estimate $\omega_{\min,\parallel} \simeq 2.5$ meV inferred from the incoherent inelastic neutron scattering data.

The molecules are approximated as spheres, which is a fair leading approximation for temperatures above 20 K where they are rotationally disordered. The venerable Lennard-Jones (12,6) functional form is used for the molecule-molecule pair potential at separation r with energy minimum at $r = R_{\min}$,

$$\phi(r) = 4\epsilon[(\sigma/r)^{12} - (\sigma/r)^6] = \epsilon[(R_{\min}/r)^{12} - 2(R_{\min}/r)^6] \tag{3}$$

with two sets of parameters: $\epsilon = 137$ K and $\sigma = 3.6814$ Å, used by Phillips[27] (JMP) in many calculations for CH_4/graphite, and $\epsilon = 148.9$ K and $\sigma = 3.783$ Å, used by Lynden-Bell[28] (RLB) in a simulation of CH_4/MgO(001) multilayers and based on a fit[29] to a range of 3D gas phase data. Given the large σ difference of 0.1 Å, it is surprising that the results of the two sets for the dense phase conditions of the monolayer do not lead to large differences in the inferred values of V_0 and V_{g0}. This may be because the intrinsic length scales of the two models span the range of physical separations that dominate the present applications, see Table I. The JMP set reproduces properties of the monolayer and bilayer solids somewhat better.

The MgO substrate is the source of a molecule-substrate van der Waals potential $V_{\rm vdW} \simeq -C_3/z^3$, $C_3 = 0.313$ a.u., and of a substrate-mediated molecule-molecule interaction. The substrate-mediated interaction in the monolayer is taken to be the McLachlan energy[30] with coefficients $C_{s1} = 47.6$; $C_{s2} = 19.0$ (atomic units) and an effective distance to the substrate (image plane) $L_{ov} = 2.25$ Å derived from the empirical CH_4-MgO distance[2,3,31] 3.30 Å. The McLachlan energy is used only for the monolayer molecules and the van der Waals potential is used for the molecules in the upper layer of the bilayer.

TABLE I. Zero-temperature properties of CH_4 and CD_4 lattices in 2D and 3D. LJ(12,6) models augmented with McLachlan (McL) or triple-dipole (td) energy as stated. Ground-state energies in K (with 3D zero-point energy) and unconstrained lattice constants (zero pressure, zero spreading pressure) in Å. $\omega_\perp = 7.5$ meV for CH_4/MgO and 6.7 meV for CD_4/MgO. Calculated lengths determined to ±0.005 Å.

species LJ	CH_4 JMP[a]	CH_4 RLB[b]	CD_4 JMP	CD_4 RLB
L_u(2D)(McL)	4.215	4.320	4.205	4.310
$E_0(\triangle)$(McL)	−305.4	−348.4	−316.1	−359.3
L_u(2D)(no McL)	4.185	4.295	4.175	4.285
$E_0(\triangle)$(no McL)	−350.3	−388.9	−361.3	−400.1
L_0 (3D) (no td)	4.095	4.20	4.085	4.195
E_0(3D) (no td)	−1006	−1104	−1021	−1119
L_0 (3D) (td)[c]	4.15	4.245	4.14	4.235
E_0(3D) (td)[c]	−909.5	−1026	−922.6	−1040
L_0(3D) (expt)[d]	4.16	...	4.14	...
E_0 (3D) (expt)[d]	−1126	...	−1156	...

[a]Phillips[27] parameters: $\epsilon = 137$ K and $\sigma = 3.6814$ Å.
[b]Lynden-Bell[28,29] parameters: $\epsilon = 148.9$ K and $\sigma = 3.783$ Å.
[c]Triple dipole strength[32] $\nu = 1680$ a.u.
[d]From data assembled in Ref. 30.

Zero-point energy causes a 2% dilation of the ground-state lattice constants of the intrinsic monolayer triangular lattice and the 3D solid and is included in all the results presented here. The 3D solid is significantly dilated by the triple-dipole (three-molecule, non-pair-additive) dispersion energy[32] as shown in Table I. Since the goal of the calculations is to determine relative stability of film structures, the emphasis is on relative energies and some of the defects of the models in giving total energies may be offset in the differences.

The structures that are treated are (1) the commensurate $c(2 \times 2)$ monolayer, (2) the commensurate $c(2 \times 2)$ bilayer, (3) the modulated triangular incommensurate monolayer both at the minimum energy lattice constant (L_u) and under compression, and (4) the heavy wall (HW) uniaxially incommensurate monolayer[7] obtained by compression of the $c(2 \times 2)$ monolayer. Structures (1) and (2) are analogous to the (1×1) lattices treated[6] for Kr/NaCl(001), while (3) is approximated as described in the Appendix. (4) is a structure that may be accessed[7] for CH_4/MgO(001) but does not arise for Kr/NaCl(001). The transitions (1) → (2) and (1) → (3) are first order transitions while (1) → (4) is continuous.

The stability determinations use the grand potential Φ of N molecules adsorbed on an area A at temperature T and chemical potential μ:

$$\Phi = N(f - \mu), \tag{4}$$

where f is the Helmholtz free energy per molecule. Φ plays the role of a generalized pressure for commensurate lattices. In the static lattice approximation, f reduces to the potential energy; when there are significant zero-point energies, the zero-temperature theory replaces f by the ground-state energy. If the monolayer solid is a commensurate square lattice, the chemical potential at monolayer condensation is $\mu_1 = E_1(\square)$. The chemical potential at condensation of a commensurate square bilayer solid is

$$\mu_2 = 2E_2(\square) - E_1(\square)\,, \tag{5}$$

and the difference is

$$\Delta\mu_{12} = \mu_2 - \mu_1 = 2[E_2(\square) - E_1(\square)]\,. \tag{6}$$

The question of whether the $c(2 \times 2)$ monolayer lattice is compressed to a triangular monolayer lattice, with area/molecule $a_x = x(2\ell^2)$, before the bilayer forms is governed by

$$\mu(x) - \mu_1 = \frac{1}{1-x}[E_1(x) - E_1(\square)]\,. \tag{7}$$

The threshold value $\Delta\mu(\triangle) \equiv \mu_1(\triangle) - \mu_1(\square)$ is the minimum of Eq. (7) as a function of x; the energy $E_1(x)$ is evaluated as described in the Appendix using a generalization of the Novaco-McTague perturbation theory[9] for the modulation energy arising from the substrate corrugation. The threshold $\Delta\mu(\mathrm{HW}) = \mu_1(\mathrm{HW}) - \mu_1(\square)$ is evaluated from the slope with misfit of the energy $E_1(\mathrm{HW})$ of a series of uniaxially

incommensurate heavy wall (HW) lattices[7] at misfits less than 1%.

The energies that are first formed in the calculations do not include the average first layer molecule-substrate energy V_0. These are denoted $\tilde{E}_1(\square)$, $\tilde{E}_2(\square)$, $\tilde{E}_1(\triangle)$, and $\tilde{E}_1(\mathrm{HW})$ and are related to the energies that enter in Eqs. (5)–(7) by

$$E_1(\square) = \tilde{E}_1(\square) + V_0, \tag{8}$$

$$E_2(\square) = \tilde{E}_2(\square) + \tfrac{1}{2}V_0, \tag{9}$$

$$E_1(\triangle) = \tilde{E}_1(\triangle) + V_0, E_1(\mathrm{HW}) = \tilde{\mathrm{E}}_1(\mathrm{HW}) + \mathrm{V}_0. \tag{10}$$

Hence $\Delta\mu(\triangle)$ and $\Delta\mu(\mathrm{HW})$ do not depend on V_0 but $\Delta\mu_{12}$ does. It is significant that the chemical potential μ_2 does not depend explicitly on V_0:

$$\mu_2 = 2\tilde{E}_2(\square) - \tilde{E}_1(\square). \tag{11}$$

Equation (11) expresses the fact that the chemical potential at bilayer condensation is insensitive to the binding of the monolayer to the substrate. This has been noted[33] for the bilayer condensation of xenon on several substrates (the C_3 term, though, does depend on the substrate). For the commensurate square lattices, the classical registry energy of $4V_{g0}$ for first layer molecules also cancels from μ_2, but V_{g0} does affect the zero-point energy in μ_2.

IV. COMPUTATIONS

The zero-point energy and free energy of the monolayer and bilayer lattices are evaluated with quasiharmonic lattice dynamics.[30,34] Calculations[27] for methane/graphite suggest this accurately includes thermal effects at temperatures below 30 K. The pair potentials are summed over seven neighbor shells in-plane ($R_c = L_{\mathrm{nn}}\sqrt{10}$) and five shells between planes for the square lattices and five shells in-plane ($R_c = 3L_{\mathrm{nn}}$) for the triangular lattice. For the methane 3D fcc lattice results in Table I, the lattice sums are cut off at a distance $R_c = 3.5L_{\mathrm{nn}}$ and the Brillouin zone sums are evaluated with the Chadi-Cohen[35] special point set.

Results for the monolayer and bilayer solids of CH_4 and CD_4 are presented in Table II for the JMP and RLB parameters. More extensive data, for several other values of Ω and for models that do not include the McLachlan interaction, are given in Supplementary Material.[10] These are zero-temperature results that include zero-point energies. For comparison, the lattice constant that minimizes the total potential energy for a 2D triangular lattice with LJ(12,6) pair potentials is $L_{\mathrm{nn}}/\sigma = 1.111$ or 4.09 Å for the JMP parameters (with −463 K cohesive energy) and 4.20 Å (with −504 K cohesive energy) for the RLB parameters. The entries for L_u in Table I, with zero-point energy but without the McLachlan energy, are 2% larger.

The entries in Table II are as follows. The frequencies ω_{min} and ω_{max} are the minimum and maximum in-plane frequencies of the $c(2\times2)$ monolayer. L_u and $\tilde{E}_u$ denote the average nearest-neighbor spacing and energy of the minimum energy modulated incommensurate triangular lattice. $\tilde{E}_1(\square)$ and $\tilde{E}_2(\square)$ denote the energy per molecule of the $c(2\times2)$ monolayer and bilayer solids. $\Delta\mu(\triangle)$ is obtained using Eq. (7), while $\Delta\mu(\mathrm{HW})$ uses data for the HW lattice at small misfit, as described there. When $\Delta\mu(\mathrm{HW}) < \Delta\mu(\triangle)$, as occurs for the larger values of Ω, the heavy wall lattice is more stable than the triangular incommensurate monolayer. The values V_0 and μ_1 are obtained from the empirical $\Delta\mu_{12} = 270$ K, using Eqs. (6), (8), and (9).

TABLE II. Zero-temperature properties of CH_4/MgO(001) and CD_4 structures with LJ parameters of Phillips[27] (denoted JMP) and Lynden-Bell[28] (denoted RLB). Calculations include the McLachlan energy and the 3D zero-point energies. $\tilde{E}_1$ and $\tilde{E}_u$ are without V_0, $\tilde{E}_2$ is without $V_0/2$, see Eqs. (8)–(10).

species LJ	CH_4 JMP	CH_4 RLB	CD_4 JMP	CD_4 RLB
Ω[a] (meV)	3.00	3.00	2.50	2.50
$2\lvert V_{g0}\rvert$ (K)	90.1	90.1	78.3	78.3
ω_{min}[b] (meV)	2.73	2.38	2.24	1.89
ω_{max}	6.65	8.47	5.87	7.51
$L_u(\triangle)$[c] (Å)	4.28	4.37	4.25	4.34
$\tilde{E}_u(\triangle)$ (K)	−324	−364	−330	−371
$\tilde{E}_1(\square)$[d] (K)	−392	−427	−380	−416
$\tilde{E}_2(\square)$ (K)	−689	−753	−688	−753
$\mu_1(\triangle) - \mu_1(\square)$[e] (K)	470	578	348	424
$\mu_1(\mathrm{HW}) - \mu_1(\square)$[f] (K)	418	540	346	406
V_0[g] (K)	−864	−921	−886	−944
μ_1 (K)	−1256	−1348	−1266	−1360

[a] Ω in terms of V_{g0}, see Eq. (2).
[b] Minimum and maximum in-plane frequencies of the $c(2\times2)$ monolayer.
[c] Average nearest-neighbor spacing and energy of the minimum energy modulated incommensurate triangle lattice, see the Appendix.
[d] Ground-state energies of the monolayer and bilayer commensurate square lattices, see Eq. (5).
[e] Chemical potential increment for compression from square to triangular monolayer lattice, see Eq. (7).
[f] Chemical potential increment for compression from square to uniaxially incommensurate heavy wall (HW) lattice, see discussion at Eq. (7).
[g] $V_0 = 2[\tilde{E}_2(\square) - \tilde{E}_1(\square)] - \Delta\mu_{12}$, using the empirical CH_4 value $\Delta\mu_{12} = 270$ K for both species.

An attempt was made to estimate the role of thermal effects at higher temperatures, because most of the data on adsorption energies is taken at relatively high temperatures, 70–90 K. This is not routine to do with the quasiharmonic theory because, as found in other monolayer and bilayer calculations, the quasiharmonic approximation leads to supra-linear thermal expansion for CH_4 at temperatures above 40 K as well as a large increase of the interplanar spacing of the bilayer. Quantum corrected cell model calculations of the unconstrained thermal expansion and $\Delta\mu(\triangle)$ are stable up to about $T = 50$ K and indicate that the thermal effects may reduce the values of $\Delta\mu(\triangle)$ relative to the $T = 0$ K values in the Tables by 20–30 K for the temperature range $T = 30$–60 K. This is not large enough to cause qualitative changes in the stability tests.

V. DISCUSSION

Requiring that the minimum in-plane phonon energy of CH_4 be $\omega_{\mathrm{min},\parallel} \simeq 2.5$ meV sets $\Omega \approx 2.8$ meV for the Phillips model and $\Omega \approx 3.0$ meV for the Lynden-Bell model. Both give values of $\Delta\mu(\mathrm{HW})$ and $\Delta\mu(\triangle)$ that are much larger

than the value $\Delta\mu_{12}$ set for the monolayer square to bilayer square transition. The calculations for CD_4, with the same value of V_{g0}, show that the square monolayer is succeeded by the square bilayer too. A separate calculation that shows the bilayer square is stable relative to the bilayer triangular lattice increases the requirement on Ω to the range 3.0–3.1 meV.

As in the modeling[6] of $p(1 \times 1)$Kr/NaCl(001), the $c(2 \times 2)$ square commensurate lattice at small corrugations V_{g0} is dynamically unstable relative to a deformation to a square commensurate Bravais lattice with four molecules in the unit cell and then $\Omega \neq \omega_{0\|}$. The threshold corrugation to make the potential energy of the one-molecule unit cell lower than that of the four-molecule CH_4 cell is $2|V_{g0}| \simeq 15$ K, i.e., $\Omega \simeq 1.2$ meV for the JMP parameters. For the RLB parameters, the values are $2|V_{g0}| \simeq 33$ K and $\Omega \simeq 1.8$ meV. Hence the four-molecule unit cell is excluded by the datum $\omega_{\min,\|} \simeq 2.5$ meV.

To make the energy of the square $c(2 \times 2)$ CH_4 monolayer lower than that of a modulated triangle, $E_1(\square) - E_u(\triangle) < 0$, requires $\Omega \geqslant 2.25$ meV and that is satisfied by the fit to $\omega_{\min,\|}$. The most severe constraint is that the chemical potential increment $\Delta\mu$ for compression from the monolayer square to other monolayer lattices ($\triangle$ and HW) must be larger than 270 K, and that requires $\Omega > 2.75$ meV. With $\Omega \simeq 3.0$ meV, the calculated gap is $\omega_{\min,\|} \simeq 2.4$–$2.7$ meV and compression of the $c(2 \times 2)$ monolayer leads to the bilayer solid and not to an incommensurate monolayer solid.

The larger core radius σ in the RLB set leads to stronger repulsive forces in the dynamics of the monolayer square lattice. The width of the in-plane phonon density of states $\omega_{\max} - \omega_{\min}$ for CH_4 is about 4 meV for the JMP set and is close to 6 meV for the RLB set. The latter width is closer to what is shown in Fig. 1. A reservation on the significance of this comparison is that the models do not treat the librational degrees of freedom of the molecule and thus the calculation omits some higher frequency motions that may be accessed in the experiments. Also, Fig. 2, the overall shape of the calculated incoherent inelastic spectrum for the RLB set is further from the experimental data than that of the JMP set.

The calculated powder-averaged incoherent inelastic neutron scattering spectrum from $c(2 \times 2)CH_4/MgO(001)$ is shown in Fig. 2 for the JMP and RLB parameter sets, both with $\Omega = 3.0$ meV. The one-phonon inelastic double-differential cross-section[36] is evaluated for initial wave number $k_i = 2.958$ Å^{-1}, wave number transfer $Q = 2.35$ Å^{-1}, target temperature 9.0 K, and a Gaussian instrumental resolution function with FWHM = 0.6 meV. The quantity shown is $D(E)$, an average density of states related to the partial differential cross section and the incoherent one-phonon spectral density $S_{\text{incoh},1}$ by

$$D(E) = \left\langle \frac{d^2\sigma}{d\omega dE'} \middle/ (\sigma_i/4\pi) \right\rangle = \langle (k_f/k_i) S_{\text{incoh},1}(Q, \Delta E) \rangle, \tag{12}$$

where σ_i is the neutron-molecule incoherent scattering cross section. The calculated spectra have two peaks, at energy transfers close to $\omega_{\min,\|}$ and $\omega_\perp$, and are in qualitative agreement with the experimental spectrum, Fig. 1. The ratio of the lower energy peak intensity to that at the higher energy

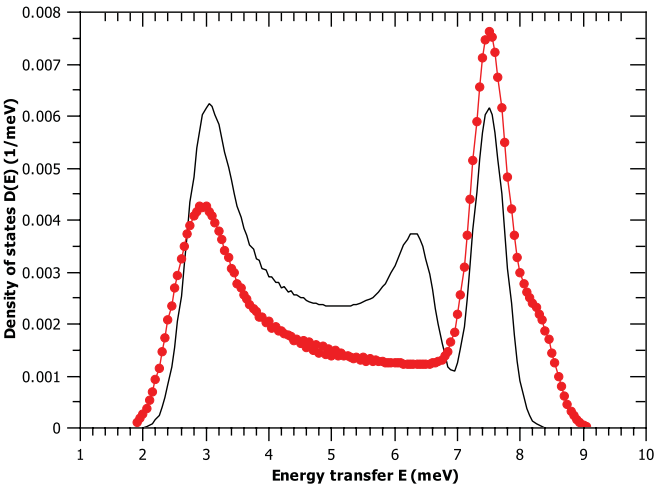

FIG. 2. (Color online) Calculated powder average of the double-differential cross section for incoherent inelastic neutron scattering from the $c(2 \times 2)$ $CH_4/MgO(001)$ monolayer, with parameters given in Sec. V and corresponding to the data in Fig. 1. The density of states function $D(E)$ defined in Eq. (12) is shown as a function of energy transfer E. The smooth and chain lines are the results for the Phillips and Lynden-Bell parameter sets, respectively, both using $\Omega = 3.0$ meV.

is about 1.5 in the experimental spectrum, about 1 for the JMP parameters, and about 0.5 for the RLB parameters.

Combining μ_2 from Eq. (11) and the $\Delta\mu_{12} \simeq 270$ K fitted to the Freitag-Larese data[12] leads to values for the monolayer condensation chemical potential at $T = 0$ K of $\mu_1 = -1256$ K for the JMP set (methane/graphite) and $\mu_1 = -1348$ K for the RLB set (methane/MgO multilayers). The offset from the 3D solid ground-state energy (including triple dipole energies) then is $\mu_1 - \mu_{3D} \simeq -350$ K for the former and $\mu_1 - \mu_{3D} \simeq -320$ K for the latter. Both values are in remarkable agreement with the estimate $\mu_1 - \mu_{3D} \simeq -350$ to -370 K from the Freitag-Larese isotherms at higher temperatures. Without the triple dipole energy in the 3D calculation, the calculated differences would have shifted by about 100 K.

The calculations[10] show that μ_1 for CH_4 varies by only 1 K as Ω is changed from 2.25 to 3.25 meV for the JMP parameters (from 2.5 to 3.25 meV for the RLB parameters). Thus μ_1 is insensitive to the value of Ω and to whether the McLachlan energy term is included, in accord with the discussion of Eq. (11).

The monolayer registry energy at $\Omega = 3.0$ meV is $-4|V_{g0}| = -180$ K. This also is the barrier to motion on the surface in a 2D model. It is smaller than an activation energy $\Delta E \simeq 660$ K fitted to the diffusion coefficient of a dense monolayer fluid of $CH_4/MgO(001)$ measured[37] by quasielastic neutron scattering for temperatures of 88 to 97 K. However, it does offset the reduction of lateral energy in the square lattice, which is approximately the $\epsilon = 137$–149 K of the Lennard-Jones (12,6) potential. The *a priori* calculations of relative site energies by Drummond *et al.*[2] give energy differences on this scale, but also show the complexity of the full molecular problem. The energy difference for the dipod orientation (edge down) at the O^{2-} and Mg^{2+} sites is 6.5 meV (75 K) with a height difference of 0.5 Å. The energy difference for the tripod down configuration is 14.2 meV (165 K) with a

height difference of 0.3 Å. The energy barrier for translational motions must be an average of these increments that arises from coupled orientational and out-of-plane motions of the molecule. The *a priori* calculations have not evaluated this yet.

The negative dispersion of the in-plane shear mode frequency from Brillouin zone center to the zone boundary is a characteristic of the square lattice. The net shift for atomic/molecular mass m is given in terms of the nearest-neighbor force and the dipole-dipole and dipole-quadrupole dispersion energy coefficients[38] C_6 and C_8 by

$$m\left[\omega^2_{\min,\parallel} - \omega^2_{0,\parallel}\right] = \frac{8}{r}\frac{d\phi}{dr}\bigg|_{r=L_{\rm nn}} - \frac{4C_6}{L^8_{\rm nn}}\left[\frac{9}{4} + \frac{312}{3125}\right] - \frac{4C_8}{L^{10}_{\rm nn}}\left[2 + \frac{560}{15625}\right], \tag{13}$$

where the first term in each square bracket on the right-hand side is the contribution of the next-nearest neighbors at distance $L_{\rm nn}\sqrt{2}$ and the second term is the contribution of farther neighbors at separations out to $L_{\rm nn}\sqrt{5}$. Equation (13) can be used to interpret the lattice dynamics calculation of the dispersion. For Kr/NaCl(001), the first term on the right-hand side is well determined from dimer spectroscopy and accurate values are available for the dispersion force coefficients C_6 and C_8 that give the dominant contributions from farther neighbors. For CH_4/MgO(001), the C_6 coefficient is believed to be known to 5%, while the accuracy of C_8 is at the 10–15% level and the nearest-neighbor term is an estimate based on spherical molecule approximations. For the Kr case,[6] with $L_{\rm nn} < R_{\rm min}$, all terms are of the same sign and the net reduction may be as large as 50% of $\omega_{0\parallel}$. For CH_4 with the JMP parameters, the first term on the right-hand side is positive ($L_{\rm nn} > R_{\rm min}$) and there is an offsetting effect. For CH_4 with the RLB parameters, the first term on the right-hand side is negative ($L_{\rm nn} < R_{\rm min}$) and the net reduction is larger.[39]

VI. CONCLUSION

The calculated stability margins between candidate dense molecular packings, once the internal parameters are optimized, tend to be a small part of the total energy and one that is hard to match reliably to experiments. However, the difference in coordination between the square and triangular lattices has large enough effect that the requirements on the external potential can be estimated rather easily. The conclusion of this paper is that the condensation of the methane monolayer as a simple commensurate square lattice that is succeeded by a commensurate square bilayer lattice is understood and consistent with the scattering and isotherm data. The observed frequency gap is large enough to require a substrate corrugation, with $\Omega \approx 3$ meV, that suffices to stabilize the observed square lattices. It is a novel situation to unite the two complementary approaches in a consistent picture.

ACKNOWLEDGMENTS

The neutron scattering work (JZL) was made possible by the generous support of the US DOE office of Basic Energy Science who operate the US neutron scattering facilities where this work was performed, the US NSF under award DMR-0412231 and a fellowship from the Joint Institute of Neutron Scattering (JINS).

APPENDIX: VARIATIONAL APPROXIMATION TO THE NOVACO-MCTAGUE ENERGY

An incommensurate monolayer solid is modulated by the spatially periodic terms in the adatom-substrate potential energy $v(\mathbf{r})$, i.e., the corrugation energy terms. Novaco and McTague[9] found that the corresponding shift ΔE of the ground-state energy often is well approximated by a second-order perturbation theory. When the corrugation is strong, as for Kr/NaCl(001) and CH_4/MgO(001), the second-order perturbation theory for ΔE leads to a divergent dilation of the lattice because the harmonic adatom-adatom force constants become very small. While this artifact might be remedied by an expansion that retains higher harmonics (anharmonic perturbation theory), a variational modification of the perturbation theory is implemented here.

Let the classical potential energy for adatoms at positions $\{\mathbf{r}_j\}$ be written as

$$\Phi = \sum_i v(\mathbf{r}_i) + \sum_{i<j} \phi(|\mathbf{r}_i - \mathbf{r}_j|)\,, \tag{A1}$$

and retain only the leading shell of reciprocal lattice vectors

$$v(\mathbf{r}) = V_g \sum_{\mathbf{g}} \exp(\imath \mathbf{g}\cdot\mathbf{r})\,. \tag{A2}$$

Second-order perturbation theory for the displacements $\{\mathbf{u}_j\}$ from the positions $\{\mathbf{R}_j\}$ in the uniform triangular incommensurate lattice driven by the $v(\mathbf{r})$ gives

$$\mathbf{u}_j = -V_g \sum_{\mathbf{g}} \exp(\imath \mathbf{g}\cdot\mathbf{R}_j)\mathbf{D}^{-1}(\mathbf{g})\cdot(\imath\mathbf{g})\,, \tag{A3}$$

$$\mathbf{D}(\mathbf{g}) = \sum_j [1 - \exp(\imath \mathbf{g}\cdot\mathbf{R}_{j0})]\nabla\nabla\phi\,, \tag{A4}$$

where the tensor $\mathbf{D}$ is proportional to the dynamical matrix of harmonic lattice dynamics.

The variational theory first evaluates the potential energy, Eq. (A1), for the positions $\mathbf{r}_j = \mathbf{R}_j + f\mathbf{u}_j$ without expanding the functions v and ϕ. The scale factor f and the angle α that a primitive vector of the triangular lattice makes with a primitive vector of the square substrate lattice are variational parameters for each choice of uniform triangular incommensurate lattice $\{\mathbf{R}_j\}$. The sums in Eq. (A1) are carried over a lattice of $800 \times 800 = 640\,000$ adatoms. The potential energy Φ is minimized as a function of f and α. The lattice constant that minimizes the potential energy plus the harmonic zero-point energy of the uniform triangular lattice is denoted $L_u(\triangle)$ in the Tables and the corresponding total energy is denoted E_u. (The subscript u denotes the "unconstrained" or zero spreading-pressure lattice.) $\Delta\mu(\triangle)$ is obtained using the optimized total energy in Eq. (7).

The variational approximation coincides with the second-order perturbation result at small corrugations, and it eliminates the divergent dilation at large corrugations that was described previously[6] for Kr/NaCl(001).

*lwbruch@wisc.edu
†jzl@utk.edu

[1] M. Bienfait and J. M. Gay, *Surface Melting and Diffusion*, in *Phase Transitions in Surface Films 2*, edited by H. Taub, G. Torzo, H. J. Lauter, and S. C. Fain Jr., (Plenum, New York, 1991), pp. 307–259.
[2] M. L. Drummond, B. G. Sumpter, W. A. Shelton, and J. Z. Larese, Phys. Rev. B **73**, 195313 (2006).
[3] S. Tosoni and J. Sauer, Phys. Chem. Chem. Phys. **12**, 14330 (2010).
[4] J. P. Coulomb, K. Madih, B. Croset, and H. J. Lauter, Phys. Rev. Lett. **54**, 1536 (1985).
[5] L. W. Bruch, R. D. Diehl, and J. A. Venables, Rev. Mod. Phys. **79**, 1381 (2007).
[6] L. W. Bruch, J. Phys. Chem. A **115**, 6882 (2011).
[7] A. Patrykiejew, S. Sokołowski, and K. Binder, J. Chem. Phys. **115**, 983 (2001).
[8] J. Z. Larese, Physica B **248**, 297 (1998).
[9] A. D. Novaco and J. P. McTague, Phys. Rev. Lett. **38**, 1286 (1977).
[10] See Supplemental Material at http://link.aps.org/supplemental/10.1103/PhysRevB.85.035401 for additional tables with data from computations with other values of the corrugation parameter Ω. Results are also given for the molecule-molecule interaction model without the McLachlan term, i.e., the interaction is given by the Lennard-Jones (12, 6) potential only.
[11] J. M. Gay, P. Stocker, D. Degenhardt, and H. J. Lauter, Phys. Rev. B **46**, 1195 (1992).
[12] A. Freitag and J. Z. Larese, Phys. Rev. B **62**, 8360 (2000).
[13] K. Madih, B. Croset, J. P. Coulomb, and H. J. Lauter, Europhys. Lett. **8**, 459 (1989).
[14] J. M. Gay, J. Suzanne, and J. P. Coulomb, Phys. Rev. B **41**, 11346 (1990).
[15] D. R. Jung, J. Cui, and D. R. Frankl, Phys. Rev. B **43**, 10042 (1991).
[16] T. Meichel, J. Suzanne, and J. M. Gay, Compte Rendues Academie Sciences Paris **303**, 989 (1986).
[17] K. Madih, Thesis, Université d'Aix-Marseille II, Marseille, 1986 (unpublished).
[18] J. L. Colwell, E. K. Gill, and J. A. Morrison, J. Chem. Phys. **39**, 635 (1963).
[19] D. L. Goodstein, J. J. Hamilton, M. J. Lysek, and G. Vidali, Surf. Sci. **148**, 187 (1984); J. Krim, J. M. Gay, J. Suzanne, and E. Lerner, Journal de Physique (Paris) **47**, 1757 (1986); H. S. Nham and G. B. Hess, Langmuir **5**, 575 (1989).
[20] W. Kunnmann and J. Z. Larese, Novel Method for the Generation of Hugh Density (Pure and Doped) Magnesium Vapors which Bypass the Liquidus Phase. US Patent 6, **179**, 897 (2001).
[21] J. Z. Larese, D. Martin y Marero, D. A. Sivia, and C. J. Carlile, Phys. Rev. Lett. **87**, 206102 (2001).
[22] J. Z. Larese, T. Arnold, A. Barbour, and L. R. Frazier, Langmuir **25**, 4078 (2009).
[23] G. Bomchil, A. Hüller, T. Rayment, S. J. Roser, M. V. Smalley, R. K. Thomas, and J. W. White, Philos. Trans. R. Soc. London B **290**, 537 (1980).
[24] H. J. Lauter, V. L. P. Frank, H. Taub, and P. Leiderer, in *Proceedings of the 19th International Conference on Low Temperature Physics*, edited by D. S. Betts, Physica B **165/166**, 611 (1990).
[25] M. L. Drummond, B. G. Sumpter, W. A. Shelton, and J. Z. Larese, J. Phys. Chem. C **111**, 966 (2007).
[26] S. L. Tait, Z. Dohnálek, C. T. Campbell, and B. D. Kay, J. Chem. Phys. **122**, 164708 (2005).
[27] J. M. Phillips and M. D. Hammerbacher, Phys. Rev. B **29**, 5859 (1984); J. M. Phillips, *ibid.* **29**, 5865 (1984).
[28] R. M. Lynden-Bell, Surf. Sci. **230**, 311 (1990).
[29] A. E. Sherwood and J. M. Prausnitz, J. Chem. Phys. **41**, 429 (1964).
[30] L. W. Bruch, M. W. Cole, and E. Zaremba, *Physical Adsorption: Forces and Phenomena* (Oxford University Press, Oxford, England, 1997).
[31] J. Z. Larese, J. M. Hastings, L. Passell, D. Smith, and D. Richter, J. Chem. Phys. **95**, 6997 (1991).
[32] D. J. Margoliash, T. R. Proctor, G. D. Zeiss, and W. J. Meath, Mol. Phys. **35**, 747 (1978).
[33] L. W. Bruch, J. M. Gay, and J. Krim, Journal de Physique (Paris) **46**, 425 (1985). This also occurs for CH_4 with[12,19] $\mu_2 - \mu_{3D} = -90$ K on MgO and -80 K on graphite.
[34] S. L. Cunningham, Phys. Rev. B **10**, 4988 (1974); L. W. Bruch and M. S. Wei, Surf. Sci. **100**, 481 (1980).
[35] D. J. Chadi and M. L. Cohen, Phys. Rev. B **8**, 5747 (1973).
[36] W. Marshall and S. W. Lovesey, *Theory of Thermal Neutron Scattering*, (Oxford University Press, Oxford, England, 1971), Sec. 4.3.
[37] M. Bienfait, J. P. Coulomb, and J. P. Palmari, Surf. Sci. **182**, 557 (1987).
[38] P. W. Fowler, P. Lazzeretti, and R. Zanasi, Mol. Phys. **68**, 853 (1989); G. F. Thomas and W. J. Meath, *ibid.* **34**, 113 (1977). $C_6 = 129.6$ a.u. and $C_8 = 4121$ a.u.
[39] Scarcely any dispersion is observed for the shear horizontal mode of $p(1 \times 1)$ para-H_2/NaCl(001), less than 0.5 meV, in $\omega_{SH} \simeq 7.0$ meV, F. Traeger and J. P. Toennies, J. Phys. Chem. B **108**, 14710 (2004). This is consistent with Eq. (13), because the coefficients for H_2 are $C_6 = 4.016$ a.u. and $C_8 = 55.96$ a.u., so that $\hbar^2[(9C_6/L_{nn}^8) + (8C_8/L_{nn}^{10})/m_{H_2}] \simeq 0.9$ meV^2.